JOURNAL OF MATERIALS SCIENCE 33 (1998) 2379–2383

Single crystals of $Dy_{1-x}Gd_xVO_4$ for magnetic applications

H. KIMURA
National Research Institute for Metals, Tsukuba, Ibaraki 305-0047, Japan
E-mail: kdeo@nrim.go.jp

M. SATO
Kitami Institute of Technology, Kitami, Hokkaido 090-0015, Japan

Y. TERADA, K. SHIMAMURA, T. FUKUDA
Institute for Materials Research, Tohoku University, Sendai 980-8577, Japan

S. MIYASHITA
Mitsubishi Electric Corporation, Sagamihara, Kanagawa 229-1112, Japan

Single crystals of $Dy_{1-x}Gd_xVO_4$ with a constant diameter were grown by the Czochralski method. These single crystals are antiferromagnetic in the temperature region below 3 K. The magnetization of the single crystals which have tetragonal symmetry along the *a* and *c* axes was measured with a superconducting quantum interference device magnetometer in the paramagnetic temperature region above 3 K. The Jahn–Teller effect for the magnetization on $DyVO_4$ was weakened by the substitution. On the basis of the values of the magnetization, the magnetic entropy change along each crystal axis was estimated for the magnetic refrigeration. Single crystal $Dy_{0.75}Gd_{0.25}VO_4$ is a promising material for the magnetic refrigerants using the Carnot cycle in the temperature range between 4.2 and 20 K.

1. Introduction

Rare-earth vanadates, such as Nd:YVO_4 and Nd:$GdVO_4$, are promising materials for solid-state laser applications [1–3]. In addition, $DyVO_4$ is of interest for magnetic applications using the unique characteristics of the Dy ion [4–7] and the Jahn–Teller effect [8–11]. For example, $DyVO_4$ is used as a magnetic material to produce liquid helium (4.2 K) in a temperature region lower than 20 K by Carnot cycle magnetic refrigeration (using its paramagnetic property when a magnetic field is applied). Magnetic materials for magnetic refrigeration (magnetic refrigerants) using the Carnot cycle have to possess the following characteristics: a large magnetic entropy change, an optimum magnetic phase transition temperature (between the antiferromagnetic and the paramagnetic phases), a small heat capacity and a large thermal conductivity as an electric insulator [12]. Rare-earth garnet single crystals, such as $Gd_3Ga_5O_{12}$ and $Dy_3Al_5O_{12}$ with cubic symmetry, have been used for magnetic refrigerants [13] because of the large magnetic entropy change, and the ease of production of large-size and high-quality single crystals, together with the large thermal conductivity. However, Dy-type single crystals with a constant diameter are generally difficult to grow from melt by the Czochralski method because of the inferior thermal conduction through the crystal during the growth. In particular, single-crystal $DyVO_4$ with a constant diameter is difficult to grow. The crystal diameter fluctuated as a result of an unstable step shape growth [4]. It is reported that, for $Dy_3Ga_5O_{12}$ with a constant diameter, the fluctuation in the crystal diameter can be improved by the substitution of Gd for Dy [14]. This method is possible to apply to $DyVO_4$ [4]. Furthermore, it is essential to know the influence of the Jahn–Teller effect on $DyVO_4$ by the substitution of Gd for Dy, and in particular the anisotropy of magnetic properties (induced by the zircon-type structure with tetragonal symmetry).

In the present work, we focused on $Dy_{1-x}Gd_xVO_4$ and grew single crystals of it. The influence of the Jahn–Teller effect on $DyVO_4$ by the substitution of Gd for Dy was evaluated from the magnetization measurement. Furthermore, the anisotropy of the magnetic properties, such as the magnetization and the magnetic entropy change, was investigated with respect to their use as practical magnetic refrigerants.

2. Experimental procedures

Single crystals of $Dy_{1-x}Gd_xVO_4$ ($x = 0, 0.25, 0.5$ and 1) were grown by the Czochralski method (using a radio-frequency power supply) using an iridium crucible of 50 mm diameter and 50 mm height [4]. The starting materials were R_2O_3 (R = Dy or Gd) and V_2O_5 powders. Their purities were 99.99%. The oxide powders were heated to eliminate absorbed moisture

and gases prior to mixing. The powders were weighed, mixed, pressed and sintered at 1200 °C for 24 h in air. The crystal structure after sintering was zircon type according to the powder X-ray analysis. All crystals were grown in an Ar atmosphere. The pulling rate was 5 mm h^{-1} and the rotation rate was 5–20 rev min^{-1}. Single-crystal $GdVO_4$ along the *c*-axis was used for the seed crystal because $GdVO_4$ had a similar lattice parameter and melting point. The growth direction was the *c* axis ([0 0 1] direction).

The powder X-ray analysis was carried out at 8.5 and 20 K using powder samples (ground from single crystals) in order to check the change in the crystal structure due to the Jahn–Teller effect.

Rectangular samples, for the magnetization measurements, were prepared from the single crystals grown carefully to avoid crystal twins. Single crystals of $Dy_{1-x}Gd_xVO_4$ were so ductile that the samples of dimensions 1 mm × 1 mm × 8 mm were prepared by grinding the single crystals using abrasive papers. The long directions were the *a* and *c* axes, respectively. The magnetization measurements were performed in the temperature range from 3 to 20 K and in applied magnetic fields up to 50 kOe using a superconducting quantum interference device (SQUID) magnetometer (applying the magnetic fields parallel to each axis). A demagnetizing factor was evaluated as less than 0.02 and could be ignored. The magnetic susceptibility was deduced from the magnetization in a weak applied magnetic field below 10 kOe.

Thermal conductivity was measured by the steady-state method using the samples of dimensions 6 mm × 6 mm × 40 mm along the *c* axis (long direction) in the temperature range from 4.2 to 30 K.

3. Results and discussion

The single crystals grown were transparent and of 10–20 mm diameter and 20–50 mm length. Fig. 1 shows the relationship between the weight fraction of crystals on $Dy_{1-x}Gd_xVO_4$ grown before the unstable step shape growth and the Gd content, together with the same relationship for $(Dy_{1-x}Gd_x)_3Ga_5O_{12}$ for which improvement in the unstable step shape growth has already been reported [14]. For $Dy_{1-x}Gd_xVO_4$ as well as $(Dy_{1-x}Gd_x)_3Ga_5O_{12}$, the improvement also depends largely on the Gd content.

Fig. 2 shows the powder X-ray patterns at 8.5 and 20 K for $DyVO_4$. At 20 K, the 6 0 0 reflection was observed corresponding to the tetragonal symmetry whereas, at 8.5 K, the splitting from 6 0 0 to 6 0 0 and 0 6 0 reflections was observed corresponding to the orthorhombic symmetry caused by the Jahn–Teller effect at 14 K on $DyVO_4$ [8–11]. However, it is difficult to observe the Jahn–Teller effect clearly because of the small lattice parameter change in the *a* axis even for $DyVO_4$ (0.17%) [6]. Therefore, it is not practical to detect the Jahn–Teller effect using the 6 0 0 peak splitting by the powder X-ray analysis of $Dy_{0.75}Gd_{0.25}VO_4$ and of other crystals which have a higher Gd content. Therefore, we try to detect the influence of the Jahn–Teller effect by the magnetization measurement.

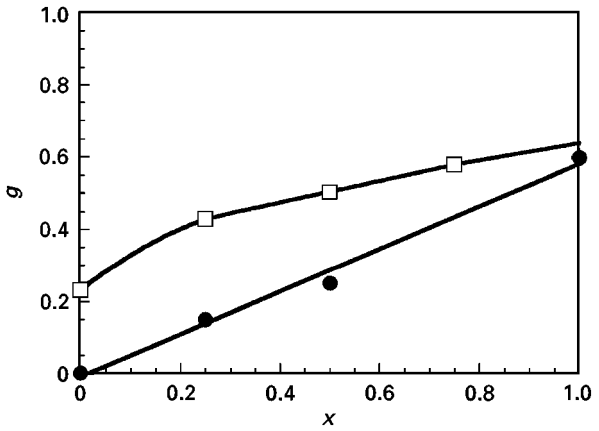

Figure 1 Weight fraction of crystal, *g*, for $Dy_{1-x}Gd_xVO_4$ (●) grown before unstable step shape growth depending on Gd content, *x*, together with *g* for $(Dy_{1-x}Gd_x)_3Ga_5O_{12}$ (□).

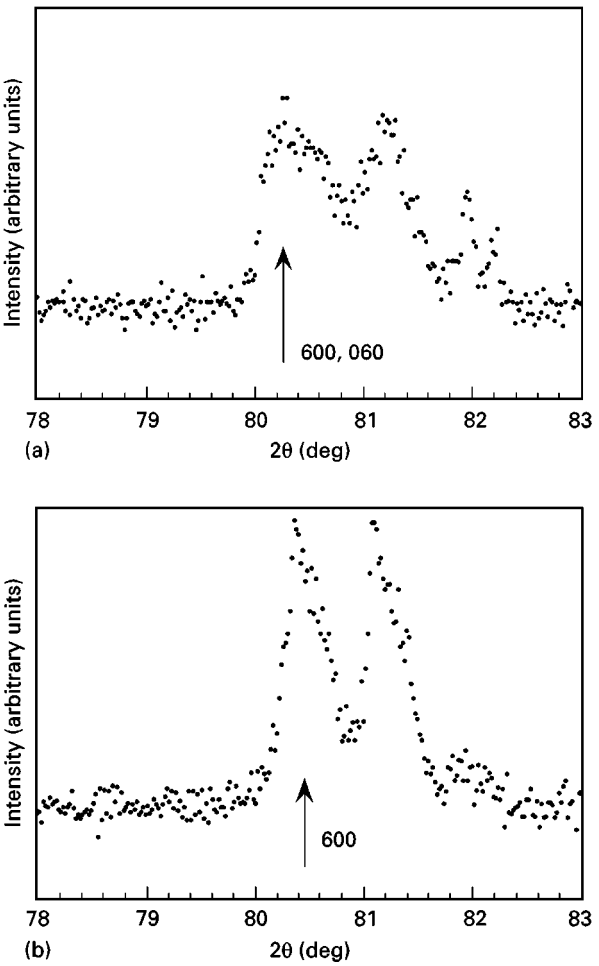

Figure 2 Powder X-ray patterns for $DyVO_4$: (a) 8.5 K; (b) 20 K.

Fig. 3 shows the temperature dependence of the magnetization, *M*, for $Dy_{1-x}Gd_xVO_4$ along each axis. There is a peak near 14 K for $DyVO_4$ along the *c* axis, but not along the *a* axis. This is because the Jahn–Teller effect reported at 14 K [8–11]. *M* along the *a* axis was 50 times that along the *c* axis in the present temperature range, so that the *a* axis was the easy-magnetization direction. This is similar to the *g* value's anisotropy of 19 (*a* axis) and 0.5 (*c* axis) below the magnetic phase transition temperature of 3 K [5, 7, 15]. For other single crystals, along both axes,

the peak was difficult to observe. The peak is observed typically for $DyVO_4$ along the c axis when M is small.

Fig. 4 shows the temperature dependence of the inverse magnetic susceptibility for $Dy_{1-x}Gd_xVO_4$.

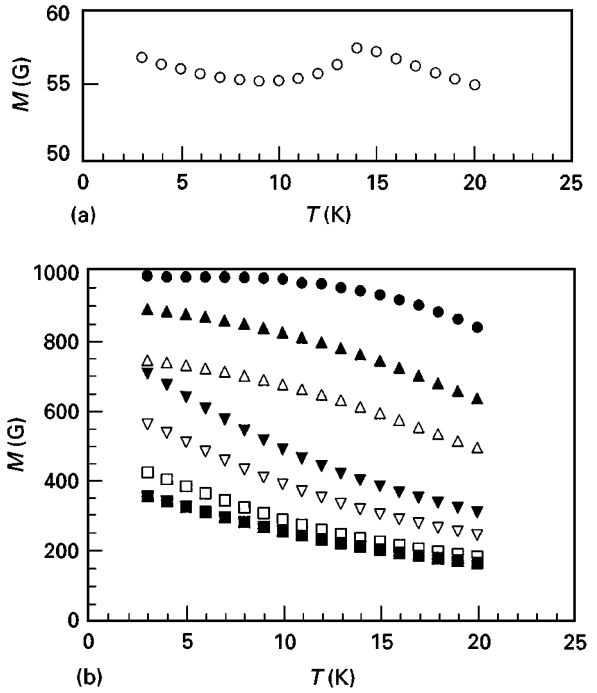

Figure 3 Temperature, T, dependence of magnetization, M, along each axis at an applied magnetic field of 50 kOe for $Dy_{1-x}Gd_xVO_4$: (a) $x = 0$ (○); (b) $x = 0$ (●), $x = 0.25$ (△, ▲), $x = 0.5$ (□, ■) and $x = 1$ (▽, ▼) . Values for both the c axis (○, △, □, ▽) and a axis (●, ▲, ■, ▼) are given.

For $Dy_{0.5}Gd_{0.5}VO_4$ and $GdVO_4$, the values obeyed the Curie–Weiss law well in the temperature region above the magnetic phase transition temperature (the Néel temperature) reported [15]. For $DyVO_4$ and $Dy_{0.75}Gd_{0.25}VO_4$, a deviation from the Curie–Weiss law was observed in a lower temperature region. This is caused by the Jahn–Teller effect because the deviation was started at 14 K for $DyVO_4$. The temperature of the Jahn–Teller effect for $Dy_{0.75}Gd_{0.25}VO_4$ is estimated as 8 K. Table I shows the paramagnetic constants for $Dy_{1-x}Gd_xVO_4$ measured above the magnetic phase transition temperature. For $DyVO_4$ and $Dy_{0.75}Gd_{0.25}VO_4$, a positive paramagnetic Curie temperature was obtained. However, we think that this is the influence of the Jahn–Teller effect. The paramagnetic Curie temperature in the present temperature range is almost negative, so that $Dy_{1-x}Gd_xVO_4$ has the antiferromagnetic properties below the magnetic phase transition temperature. The

TABLE I Paramagnetic Curie constant, C_m, paramagnetic Curie temperature, Θ_p, and magnetic moment, p, for $Dy_{1-x}Gd_xVO_4$

x	Axis	C_m (Kcm^3mol^{-1})	Θ_p (K)	P (μ_{eff})
0	a	9.2	9.3	8.6
0	c	6.2	− 95	7.0
0.25	a	12	2.2	9.8
0.25	c	9.7	0.42	8.8
0.5	a	4.0	− 2.4	5.7
0.5	c	4.3	− 2.4	5.9
1	a	7.8	− 2.9	7.9
1	c	6.1	− 3.0	7.0

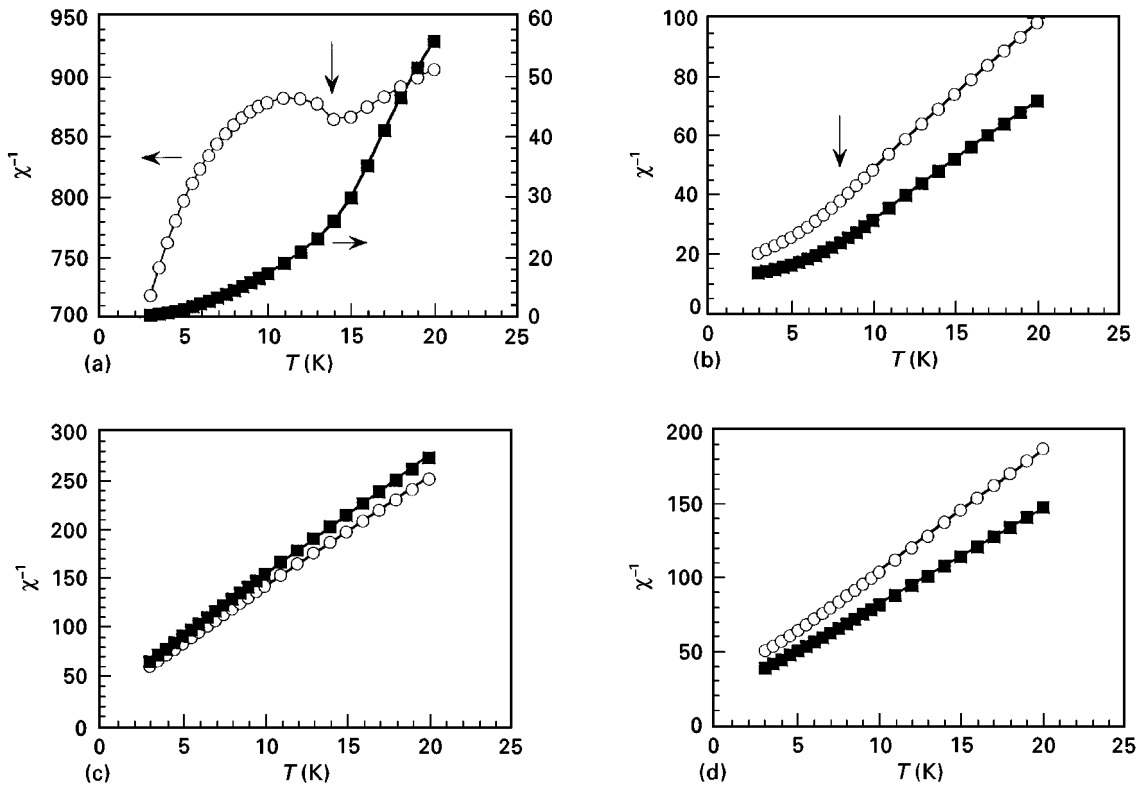

Figure 4 Temperature, T, dependence of inverse magnetic susceptibility, χ^{-1}, for $Dy_{1-x}Gd_xVO_4$: (a) $x = 0$; (b) $x = 0.25$; (c) $x = 0.5$; (d) $x = 1$. Values for both the c axis (○) and a axis (■) are given. The vertical arrows show the Jahn–Teller temperature expected.

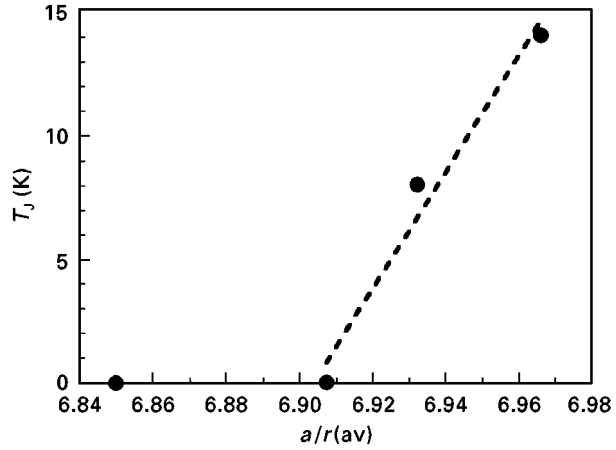

Figure 5 Relationship between the Jahn–Teller temperature, T_j, and the ratio of the lattice parameter a to the average ionic radius r (av) of rare-earth ions for $Dy_{1-x}Gd_xVO_4$, assuming $T = 0$ K at no Jahn–Teller effect.

anisotropy in magnetic properties was weakened by the increase in the Gd content.

Fig. 5 shows the relationship between the temperature of the Jahn–Teller effect and the ratio of the lattice parameter a to the average ionic radius r (av) of rare-earth ions. Here, we assume that the temperature is 0 K for $Dy_{1-x}Gd_xVO_4$ when the Jahn–Teller effect is not observed. The temperature of the Jahn–Teller effect decreased with decrease in a/M_{av} for Gd contents below 0.5.

Fig. 6 shows the temperature dependence of the magnetic entropy change, ΔS_M, calculated from the results in Fig. 3 [16]. A negative value means a decrease in ΔS_M when the magnetic field is applied. The absolute values of ΔS_M mostly decreased with increase in temperature. An anisotropic ΔS_M is observed for $Dy_{1-x}Gd_xVO_4$ (the largest is for $DyVO_4$). ΔS_M for $Dy_{0.75}Gd_{0.25}VO_4$ along both axes is large in the temperature range measured. For ΔS_M, the influence of the Jahn–Teller effect was also observed in a lower temperature region than 14 K for $DyVO_4$ and 8 K for $Dy_{0.75}Gd_{0.25}VO_4$.

Fig. 7 shows the temperature dependence of ΔS_M for $Dy_{0.75}Gd_{0.25}VO_4$ along the a axis, together with ΔS_M for $Dy_3Al_5O_{12}$ and $Gd_3Ga_5O_{12}$ along the $\langle 1\,1\,1\rangle$ direction and $DyAlO_3$ along the b axis [17]. ΔS_M for $Dy_{0.75}Gd_{0.25}VO_4$ along the a axis is superior to ΔS_M for $Dy_3Al_5O_{12}$ and $Gd_3Ga_5O_{12}$, and slightly inferior to ΔS_M for $DyAlO_3$ in the temperature range from 4.2 to 20 K.

Fig. 8 shows the temperature dependence of the thermal conductivity, λ, of the single crystals for $Dy_{1-x}Gd_xVO_4$ ($x = 0$ ($DyVO_4$) and $x = 1$ ($GdVO_4$)), together with λ for $Dy_3Ga_5O_{12}$, $(Dy_{0.5}Gd_{0.5})_3Ga_5O_{12}$ and $Gd_3Ga_5O_{12}$ single crystals along the $\langle 1\,1\,1\rangle$ direction [18]. λ is required to be above 1 W K^{-1} cm^{-1} as a criterion, according to an investigation of the magnetic refrigeration system using the Carnot cycle. For $DyVO_4$, λ is small, below 1 W K^{-1} cm^{-1}. However, it is reported for $(Dy_{1-x}Gd_x)_3Ga_5O_{12}$ as shown in Fig. 8 that λ increased with increase in Gd content caused by the decrease in the magnetic phonon scattering (induced by the Dy ion) [18]. Therefore, λ also increased with the increase in Gd content for the criterion to hold for $Dy_{1-x}Gd_xVO_4$.

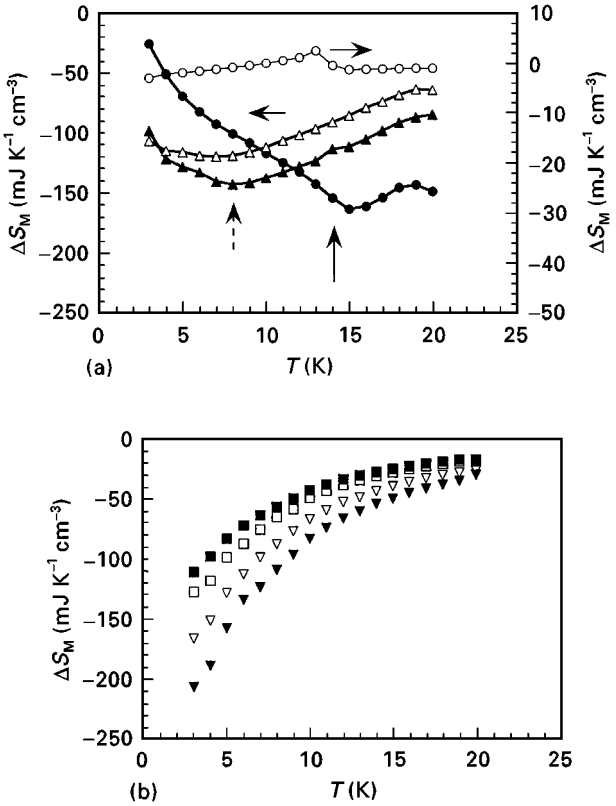

Figure 6 Temperature, T, dependence of the magnetic entropy change, ΔS_M, along the c axis (○, △, □, ▽) and a axis (●, ▲, ■, ▼) at an applied magnetic field of 50 kOe for $Dy_{1-x}Gd_xVO_4$: (a) $x = 0$ (○, ●) and $x = 0.25$ (△, ▲) ; (b) $x = 0.5$ (□, ■) and $x = 1$ (▽, ▼). The vertical arrows show the Jahn–Teller temperature expected.

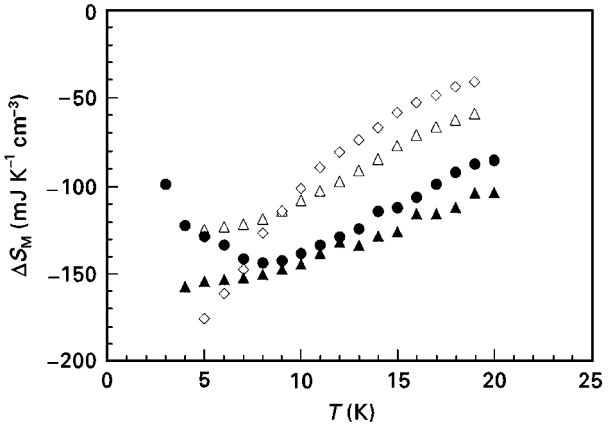

Figure 7 Temperature, T, dependence of magnetic entropy change, ΔS_M, for $Dy_{0.75}Gd_{0.25}VO_4$ (●) along the a axis, together with ΔS_M for $DyAlO_3$ (▲) along the b axis, and for $Dy_3Al_5O_{12}$ (△) and $Gd_3Ga_5O_{12}$ (◇) along the $\langle 1\,1\,1\rangle$ direction, at an applied magnetic field of 50 kOe.

According to the values of the ΔS_M and λ, $Dy_{0.75}Gd_{0.25}VO_4$ is inferior to $DyAlO_3$. However, the single crystal is easy to grow since the melting point is 1800 °C, which is lower than the melting point of 2000 °C for $DyAlO_3$. Therefore, $Dy_{0.75}Gd_{0.25}VO_4$

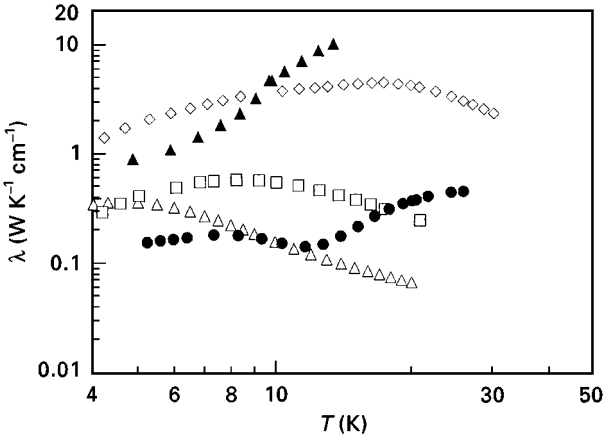

Figure 8 Temperature, T, dependence of the thermal conductivity, λ, for single crystals of $Dy_{1-x}Gd_xVO_4$ ($x = 0$ (●) and $x = 1$ (▲)) along the c axis, together with λ for $Dy_3Ga_5O_{12}$ (△), ($Dy_{0.5}Gd_{0.5}Ga_5O_{12}$ (□) and $Gd_3Ga_5O_{12}$ (◇) single crystals along the ⟨1 1 1⟩ direction.

single-crystal is useful as a practical magnetic refrigerant in order to produce liquid helium between 4.2 and 20 K using the Carnot Cycle. $Dy_{0.75}Gd_{0.25}VO_4$ single-crystal also has a Jahn–Teller effect, but the stress caused by the effect is small. That is to say, a crack was generated for $DyVO_4$ during the magnetization measurement, but not for $Dy_{0.75}Gd_{0.25}VO_4$. Therefore, $Dy_{0.75}Gd_{0.25}VO_4$ single-crystal is indeed a practical material.

4. Conclusion

Single crystals of $Dy_{1-x}Gd_xVO_4$ with tetragonal symmetry were grown by the Czochralski method. The magnetization of the single crystals along the a and c axes was measured with a SQUID magnetometer in the paramagnetic temperature region above 3 K, and the magnetic entropy change was estimated. The influence of the Jahn–Teller effect was observed but was not so effective for $Dy_{1-x}Gd_xVO_4$. According to the values of the magnetic entropy change along the crystal axis, single crystals of $Dy_{0.75}Gd_{0.25}VO_4$ along both axes were promising materials as magnetic refrigerants using the Carnot cycle magnetic refrigeration in the temperature range between 4.2 and 20 K.

Appendix

Table AI shows the lattice parameters of $Dy_{1-x}Gd_xVO_4$ [4]. Here, we adopt the conventional way to describe the crystal axis.

TABLE AI Lattice parameters of $Dy_{1-x}Gd_xVO_4$ [4]

x	Lattice parameters (nm)	
	a	c
0	0.715 46	0.631 25
0.25	0.716 83	0.631 25
0.5	0.718 38	0.631 99
1	0.721 30	0.634 88

Acknowledgements

A part of this work was performed under the Visiting Researcher's Program of the Laboratory for Development Research of Advanced Materials, Institute for Materials Research, Tohoku University.

References

1. J. R. O'CONNOR, *Appl. Phys. Lett.* **9** (1966) 407.
2. T. JENSEN, V. G. OSTROUMOV, J. -P. MEYN, G. HUBER, A. I. ZAGAMENNYI and I. A. SHCHERBAKOV, *Appl. Phys. B* **58** (1994) 373.
3. K. SHIMAMURA, S. UDA, V. V. KOCHURIKHIN, T. TANIUCHI and T. FUKUDA, *Jpn. J. Appl. Phys.* **35** (1996) 1832.
4. Y. TERADA, T. MAEDA, V. V. KOCHURIKHIN, K. SHIMAMURA, S. UDA and T. FUKUDA, *J. Cryst. Growth* **178** (1997) 518.
5. G. WILL and W. SCAFER, *J. Phys. C* **4** (1971) 811.
6. F. SAYETATAT, J. X. BOUCHERLE, M. BELAKHOVSKI, A. KALLEL, F. TCHEOU and H. FUESS, *Phys. Lett. A* **34** (1971) 361.
7. A. H. COOKE, C. J. ELLIS, K. A. GEHRING, M. J. M. LEASK, D. M. MARTIN, B. M. WANKLYN, M. R. WELLS and R. L. WHITE, *Solid State Commun.* **8** (1970) 689.
8. J. R. SANDERCOCK, S. B. PALMER, R. J. ELLIOTT, W. HAYES, S. R. P. SMITH and A. P. YOUNG, *J. Phys. C* **5** (1972) 3126.
9. R. J. ELLIOTT, R. T. HARLEY, W. HAYES and S. R. P. SMITH, *Proc. R. Soc. A* **328** (1972) 217.
10. H. UNOKI and T. SAKUDO, *Phys. Rev.* **38** (1977) 137.
11. J. B. FORSYTH and C. F. SAMPSON, *Phys. Lett. A* **36** (1971) 223.
12. H. KIMURA, *Cur. Top. Cryst. Growth Res.* **1** (1994) 329.
13. T. NUMAZAWA, H. KIMURA, M. SATO and H. MAEDA, *Cryogenics* **33** (1993) 547.
14. H. KIMURA, T. NUMAZAWA, M. SATO and H. MAEDA, *J. Cryst. Growth* **87** (1988) 523.
15. S. H. SMITH and B. M. WANKLYN, *ibid.* **21** (1974) 23.
16. T. HASHIMOTO, T. NUMAZAWA, M. SHINO and T. OKADA, *Cryogenics* **21** (1981) 647.
17. H. KIMURA, T. NUMAZAWA, M. SATO, T. IKEYA, T. FUKUDA and K. FUJIOKA, *J. Mater. Sci.* **32** (1997) 5743.
18. T. NUMAZAWA, H. KIMURA, A. SATO, H. MAEDA, K. SHIMAMURA and T. FUKUDA, *Adv. Cryog. Eng.* **42** (1996) 459.

Received 12 February 1997
and accepted 5 February 1998